Solar Panel Segmentation in High-Resolution Satellite Imagery: A YOLOv8-GIS Approach in the Marrakech-Safi Region, Morocco

Mohamed SMOUNI[1,2], Hachem SAADAOUI[2], Hassan RHINANE[1], Abdellatif GHENNIOUI[2]

[1] Geosciences Laboratory, Faculty of Sciences-Ain Chock, Hassan II University, Casablanca, Morocco
[2] Green Energy Park (GEP), Regional Road Kelaa Km 3, Benguerir, R206, Morocco

Keywords: GIS, Computer vision, Yolov8, Solar Panels, Segmentation

Abstract

Green energy usage in Morocco is gaining traction, particularly in the realm of solar panels, which hold great potential for use in agriculture and residential settings. Recently, there has been growing interest in exploring ways to automatically gather important information about solar installations in specific geographic areas of interest. To address this goal, we developed a geoAI approach that utilizes satellite high-resolution imagery and the YOLOv8 computer vision algorithm for accurate solar panel segmentation in the Marrakech-Safi region of Morocco. Training images were obtained from open-source, annotated datasets available on the web, and we pseudo-labeled images from our Area of Interest using a semi-supervised learning approach. We built, trained, and tested the solar panel dataset, which included 4660 images. Subsequently, we performed geoprocessing analysis to extract estimated geometric parameters such as the area, perimeter, and angles of the segmented solar panels. These shape parameters were then employed in unsupervised machine learning to detect anomalies in the segmented data by using the Isolation Forest algorithm. Precision, recall rate, and mAP50 were used for the evaluation of the Yolov8 segmentation model. The results showed a high precision rate of 96.9%, a recall rate of 97.6%, and an mAP score of 0.99, indicating the effectiveness of the Yolov8 segmentations in accurately segmenting solar panels. Our approach successfully segmented 18,050 PV modules, covering an estimated area of 1.47 km2 in the study area, with an average confidence of 89%. This demonstrates the model's capability to accurately identify and isolate solar panels within complex scenes. The high precision and recall rates suggest that our approach is robust for large-scale solar panel detection in diverse landscapes. Successfully segmenting over 18,000 PV modules indicates the scalability of our method. Additionally, integrating geoprocessing analysis and the Isolation Forest algorithm enhances our approach, allowing for the identification of anomalies in solar panel installations. This research provides valuable insights into the extent of solar panel adoption in the Marrakech-Safi region, offers a robust methodology for large-scale solar installation mapping, and establishes a foundation for future nationwide studies, potentially informing energy policies and supporting sustainable development initiatives across Morocco.

1. Introduction

In Morocco, there have been a lot more installations of residential and agricultural systems over the past ten years. The generated energy of solar PV systems, which was only 63 GWh in 2014, significantly increased and reached 1547 GWh in 2020 and 1848 GWh in 2021. According to the International Energy Agency, Morocco's renewable energy capacity will increase to reach 3,000 MW in 2025 (IEA, 2016). It is important to note that over the forecast period, solar PV systems will account for 14% of the nation's growth in renewable energy (Hochberg, M. 2018).
Government organizations are keen on obtaining accurate information about the location, size, and energy generation of existing solar PV installations. This data is vital for tracking the overall growth of solar systems in a particular area and making important decisions, including energy demand forecasts, development planning, distribution upgrades, and ensuring a reliable and resilient power grid. Formal data collection techniques, like surveys, take a long time and don't offer enough accuracy. Additionally, the rapid growth of residential and agricultural PV systems makes these techniques obsolete and necessitates ongoing, costly data collection efforts.

Computer vision algorithms and convolutional neural networks have shown great potential for detecting solar panels using remote sensing data. These algorithms can precisely identify and locate solar PV installations by examining high-resolution satellite imagery. Several studies have explored this approach, demonstrating promising results. For instance, Malof et al. (2015) and Hong et al. (2017) utilized computer vision techniques to detect solar PV systems from remote sensing data. Additionally, Qi Li et al. (2023) results indicate that their SolarDetector, employing the Mask R-CNN algorithm, achieved superior performance in accurately detecting rooftop solar arrays and providing detailed installation information, outperforming the notable approach of (Q. Li et al., 2020) by approximately 50%.

In the present paper, we suggest the employment of the Yolov8 segmentation model (Ultralytics, 2023), the newest deep-learning architecture from the YOLO series of frameworks (Terven, 2023). YOLO models have been widely used in remote sensing, such as in studies by Cheng et al. (2021), Alganci et al. (2020), Zheng et al. (2022), and C. Yu et al. (2023), and have made significant progress in object detection and segmentation. The YOLO family of object detection models has been renowned for its emphasis on striking the perfect balance between speed and accuracy, ensuring real-time performance without compromising on detection quality. Building upon the successes of its predecessors, the YOLOv8 model further elevates speed and accuracy, offering a unified framework for training models optimized to instance segmentation tasks (Ultralytics, 2023). Consequently, our decision to opt for YOLOv8 was clear and strategic, as we sought the ideal trade-off between high accuracy and speed. This choice is particularly crucial for us, given our

intention to utilize the model for prediction on a very large study area.

Remote sensing is a research area that requires high computation capabilities and combining it with deep learning algorithms makes the task even more demanding. Thus, many researchers have tried applying Yolov8 models to make use of its advantages in solving this problem. Ma and Pang (2023) proposed an enhanced method based on YOLOv8s. This method focuses on accurately recognizing tiny objects in remote sensing images by replacing the strided convolution module in YOLOv8s with the SPD-Conv module. In another study by Adegun et al. (2023), Yolov8 and other R-CNN algorithms were compared to detect vegetation and swimming pools in high-resolution satellite images. The results showed that Yolov8 outperformed the other methods in terms of both accuracy and speed of detection. Hajjaji et al. (2023) successfully applied Yolov8 for early detection of The Red Palm Weevil using UAV images. Their model achieved remarkable results, boasting 100% precision and recall in detecting and pinpointing infested palm trees. In summary, Yolov8 has shown promising potential in various remote sensing applications, offering improved accuracy and efficiency compared to other algorithms.

Many studies have focused on identifying solar PV locations worldwide, but there hasn't been any research done specifically for Morocco. Our study aims to address this gap by using the Yolov8 algorithm with high-resolution satellite images to precisely locate and segment solar PV installations in Morocco. This research will not only enhance our understanding of solar energy distribution in the country but also offer valuable insights for future renewable energy planning and development. To improve segmentation accuracy despite limited training samples and computational resources, we propose a geoAi approach that combines geospatial analysis and computer vision techniques. The primary objectives of this research are as follows:

1. Segmentation of PV panels and identification of their locations in georeferenced satellite imagery
2. Extract geometric parameters such as area, perimeter, and angles of the identified PV panels for further analysis and mapping purposes.
3. Using the isolation forest algorithm, perform unsupervised machine learning to use extracted shape parameters to identify anomalies and outliers in the results.

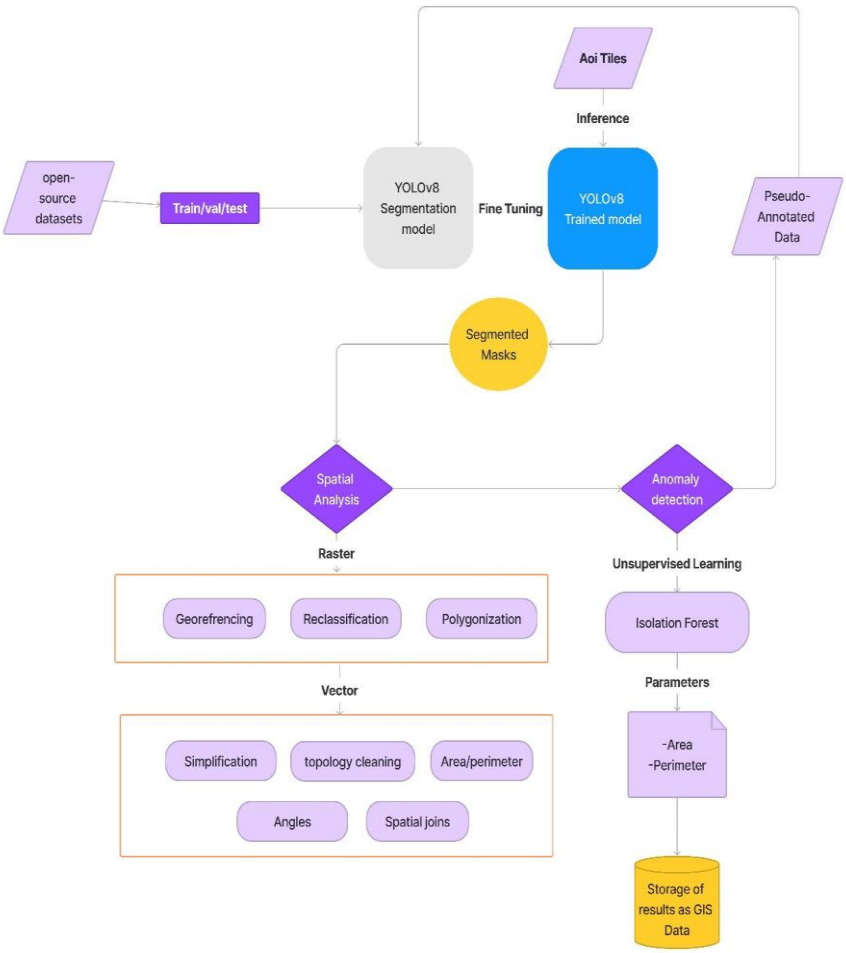

Figure 1: The methodological framework of the research.

2. Material and Methods

2.1. Study Area

This study focuses on Morocco's Marrakech-Safi region, bordered by Casablanca-Settat, Beni Mellal-Khenifra, Drâa-Tafilalet, and Souss-Massa regions, along with the Atlantic Ocean. Covering 39,167 km², it holds 115 people per sq km. With an arid climate, temperatures range from 4.9°C to 37.7°C. Notably, Marrakech-Safi boasts high direct normal irradiance (DNI) up to 3000 kWh m-2 year-1, ideal for solar PV installations.

2.2 Land Exclusion

Given the extensive expanse covered by the region (figure 2), a vital measure involved excluding land areas with a significant likelihood of lacking any photovoltaic (PV) installations. To achieve this, we leaned on the Dynamic World V1 dataset from 2022 (Brown et al., 2022), which furnished comprehensive insights into global land use and cover. This dataset facilitated precise identification of regions with minimal potential for housing PV installations. These specific regions were demarcated by distinct bands: shrub and scrub, bare land, snow and ice, as well as water bodies.

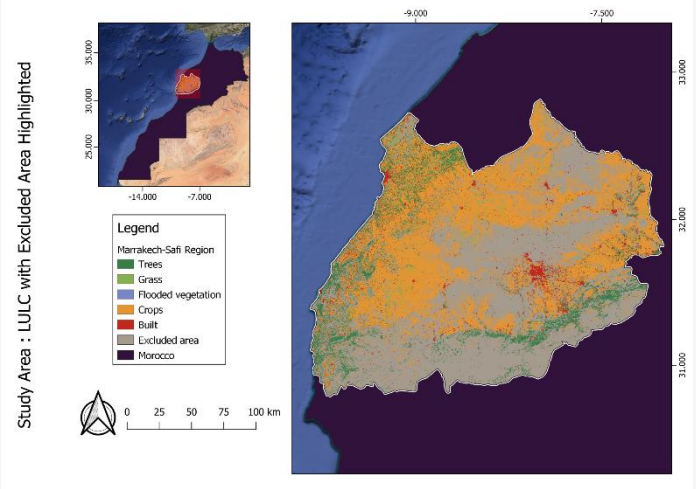

Figure 2: Study area and excluded areas highlighted.

2.3 Dataset preparation

The use of PV modules is already an established sector in agricultural and residential areas in Morocco (source). However, there is no open-source dataset of the location of PV installations in the country available to use as training samples. Therefore, we relied on open-source datasets of annotated solar panels in Satellite images available on Roboflow and Kaggle. In addition, we located a small number of PV installations in our AOI and annotated it manually. This web dataset obviously does not represent our AOI. Our goal is to use semi-supervised learning by training a Yolov8 segmentation model with the previously stated training set of data. to build a trained and tested pseudo-annotated dataset from the AOI.

Following this method, we collected high-resolution satellite imagery (0.2 m per pixel) and geospatial data (figure 3). We randomly selected samples of images from all provinces of Marrkech-Safi. Our dataset contains 4660 high-resolution pseudo-annotated images with (512 x 512) pixels and one or more agricultural or residential PV panels in each tile. Images and their annotations were split into training, validation, and test sets, with 80%, 10%, and 10% samples in each set (see table 1).

Overview	Description
Number of images	4660
Image resolution	512 x 512
Spatial resolution	0.2 - 0.5 m
Type of use	Solar panel segmentation
Data split	8:1:1

Table 1: Photovoltaic satellite image dataset.

Figure 3: Examples of collected data In Marrakech-safi region

2.4 Segmentation model

2.4.1 YOLO algorithm

Joseph Redmon and Ali Farhadi created the You Only Look Once (Yolo) object detection and image segmentation model at the University of Washington. Since the initial release of Yolo [joseeph] in 2015, changes have been made to the architecture and cost functions to increase its precision and efficiency. Yolo involves partitioning an image into a grid of smaller regions and subsequently making predictions for bounding boxes and class probabilities for each object detected within those regions.

2.4.2 YOLOv8 Segmentation model

Ultralytics, the company behind YOLOv5, launched YOLOv8. This latest release introduced five different scaled versions: YOLOv8n (nano), YOLOv8s (small), YOLOv8m (medium), YOLOv8l (large), and YOLOv8x (extra large). YOLOv8 boasts extensive capabilities, supporting various vision tasks like object detection, segmentation, pose estimation, tracking, and classification.

YOLOv8 adopts an anchor-free model featuring a decoupled head, which efficiently handles objectness, classification, and regression tasks as separate branches. This strategic design enables each branch to concentrate solely on its designated task, leading to enhanced overall model accuracy. In the output layer of YOLOv8, the activation functions chosen are significant for their respective purposes. The sigmoid function is utilized for the objectness score, indicating the likelihood that a bounding box contains an object. On the other hand, the softmax function is applied to the class probabilities, representing the likelihood of objects belonging to each potential class.

YOLOv8 offers a semantic segmentation model called the YOLOv8-seg model. The backbone is a CSPDarknet53 feature extractor, followed by a C2f module instead of the traditional YOLO neck architecture. The C2f module is followed by two semantic segmentation heads, which learn to predict the semantic segmentation masks for the input image. The model has similar detection heads to YOLOv8, consisting of five detection modules and a prediction layer. The YOLOv8-Seg model utilizes a Deconvolution module to upscale the feature maps, aligning them with the size of the input image. The resulting output from the Deconvolution module is then processed by a Softmax layer, generating a probability distribution that corresponds to the semantic labels of the input image. The model has achieved state-of-the-art results on various object detection and semantic segmentation benchmarks while maintaining high speed and efficiency.

In this study, as summarized in Table 2 , we employed the YOLOv8m-seg medium model to detect and segment the PV panels in high-resolution satellite images. a model with a size of 27.3m parameters. A pretrained model Yolov8m-seg.pt, was used for fine tuning. running on a T4 GPU provided by the Kaggle platform, for the optimizer choice In the YOLOv8 codebase, a deliberate optimization strategy is employed during training. The optimizer AdamW is initially utilized for the first 10,000 iterations, which aids in achieving faster convergence, particularly during the early training stages. However, after this initial phase, the optimizer is switched to SGD for the remaining iterations. This change is based on the observation that employing SGD for fine-tuning after a certain point can lead to improved overall performance(Ultralytics, 2023). The training of the Model spanned 120 epochs, employing a learning rate schedule that started with lr0=0.01 and linearly decreased with each epoch until it reached lrf=0.01 at the end of training. This approach ensures appropriate scaling over large batches, promoting effective model convergence while using a batch size of 24. In YOLOv8, several augmentations are applied during the training process by default with a probability of 0.01. These augmentations include Blur, MedianBlur, ToGray, and CLAHE. Additionally, YOLOv8 makes use of the mosaic augmentation technique, which combines four images into a single composite. This mosaic augmentation not only enhances the variation in the

training data but also effectively addresses the issue of overfitting, contributing to a more robust and accurate model.

Configurations and hyperparameters	Description
Segmentation model	YOLOv8m-seg
Backbone	CSPDarknet53
pre-trained weights	COCO2017
Number of classes	2 (solar panel, background)
Input image size	512 x 512
Augmentation methods	Horizontal flip, shift scale rotate.
Optimizer	Adamw, SGD
Batch size	24
Number of epochs	120
GPU	T4

Table 2. Configuration and hyperparameters specifications of yolov8.

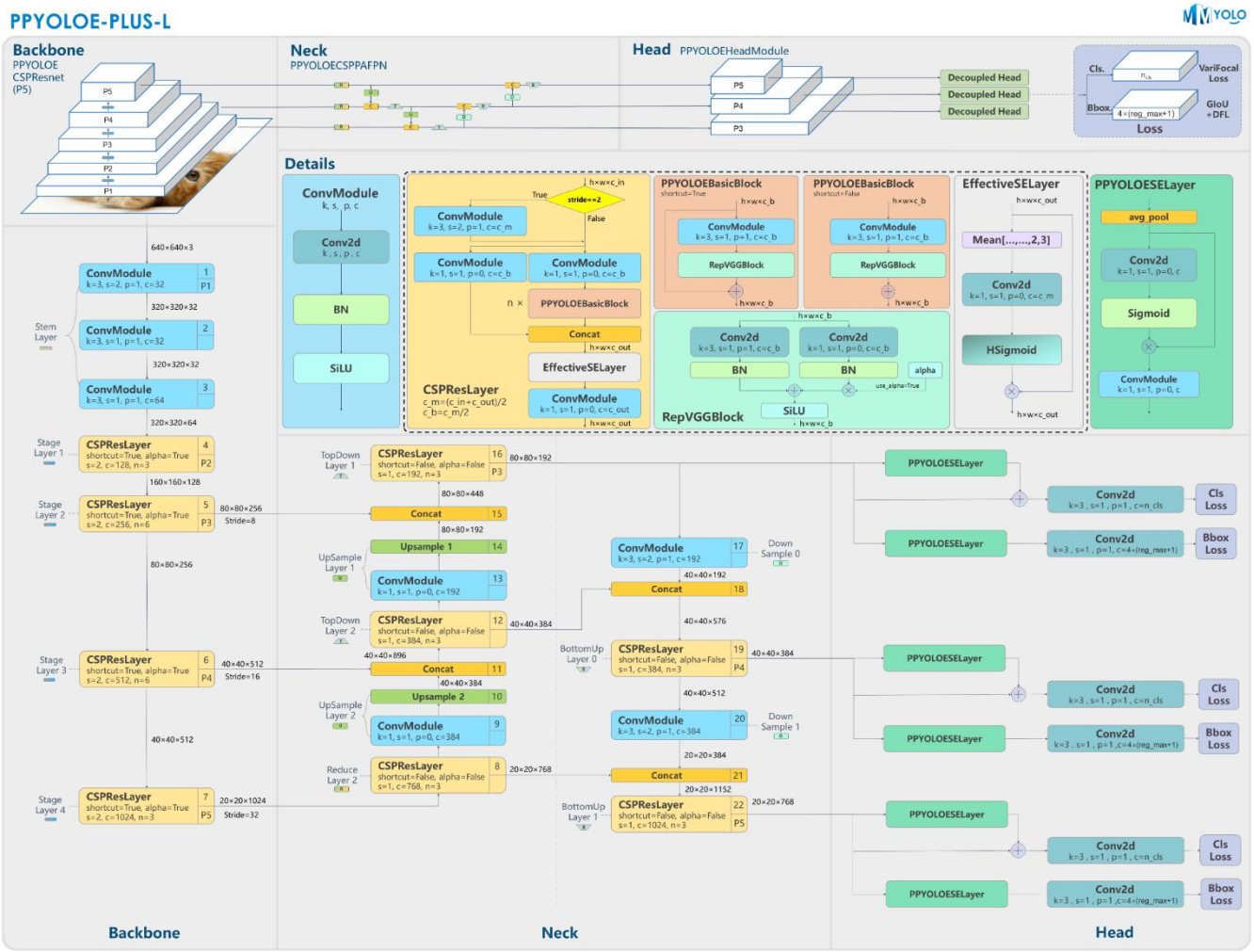

Figure 4: Brief summary of YOLOv8 model structure(Ultralytics, 2023)

2.5. Performance evaluation

In YOLOv8-seg, a combined loss function is employed, incorporating three key components: bounding box loss, objectness loss, and segmentation loss. This integrated approach allows the model to efficiently perform both object detection and semantic segmentation tasks simultaneously. The loss calculation involves classification and regression branches, with the classification branch utilizing BCE Loss and the regression branch using a combination of DFL and CIoU Loss. The specific choice of loss functions is influenced by factors such as the task's nature and the model's configuration. While BCE, DFL, and CIoU loss functions are commonly used, they can be automatically adapted or substituted based on the problem. The following performance metrics are also used to evaluate accuracy.

- Precision: Precision measures the proportion of positively predicted samples that truly belong to the positive class (Olson David and Delen, 2008).

$$Precision = \frac{TP}{TP + FP}$$

- Recall: Recall quantifies the proportion of positive examples in the dataset that are correctly predicted as positive class (Olson David and Delen, 2008).

$$Recall = \frac{TP}{TP + FN}$$

Where:
TP: True positive
FN: false negativce
FP: false positive

- mAP50: mAP50 denotes the mean Average Precision at an IoU threshold of 0.50, which assesses the model's segmentation performance (intersection over union) for moderate alignment with ground truth bounding boxes and mask.
- Intersection-over-Union (IoU), alternatively known as the Jaccard Index, is computed by dividing the shared area between the predicted segmentation and the ground truth by the combined area of the two (Taha and Hanbury, 2015).

$$IoU = \frac{TP}{TP + FP + FN}$$

2.6 Geospatial processing and analysis

Solar PV segmentation was accomplished through computer vision techniques. To leverage the outcomes, Geographic Information Systems (GIS) played a crucial role. We executed a sequence of geospatial processes to properly georeference and reclassify the generated masks. Subsequently, we converted them into polygons. These procedures enable us to conduct a variety of additional geospatial analyses with the segmented solar PV data. Georeferencing masks utilized the Rasterio (2013) library. Spatial metadata was transferred from the original 512x512 tile to its corresponding mask. Reclassification in Rasterio assigned no data to zero-value pixels. This enabled accurate polygonization of PV masks using the Shapely library, extracting valid shapes from the raster as vector polygons. Additionally, QGIS was employed to simplify polygon geometry by reducing vertex count through the Douglas-Peucker algorithm (Wu & Márquez, 2004). This process led to an improved PV data representation; we reprojected vector polygons to the local Coordinate Reference System (ESPG:26191). to ensure precise calculations of area and perimeter using QGIS. We made use of GeoPandas for spatial joins, assigning attribute data for provinces and communes to each polygon.

2.7 Anomaly detection

We employed the Isolation Forest (iForest) algorithm (F. Liu et al., 2008), a robust unsupervised learning technique explicitly designed to isolate anomalies within our results. This algorithm excels at identifying and highlighting unusual data points by isolating them from the rest of the dataset. In our analysis, we focused on solar panel polygons, utilizing their area and perimeter as essential parameters. To enhance the precision of our anomaly detection, we set an anomaly contamination rate of 0.05, enabling us to pinpoint potential irregularities with greater precision.
The anomaly score s of an instance x is defined as:

$$S(x,n) = 2^{-\frac{E(h(x))}{c(n)}}$$

where h(x) is the path length and E(h(x)) is the average of h(x) from a collection of isolation trees, c(n) is the average of h(x) given n

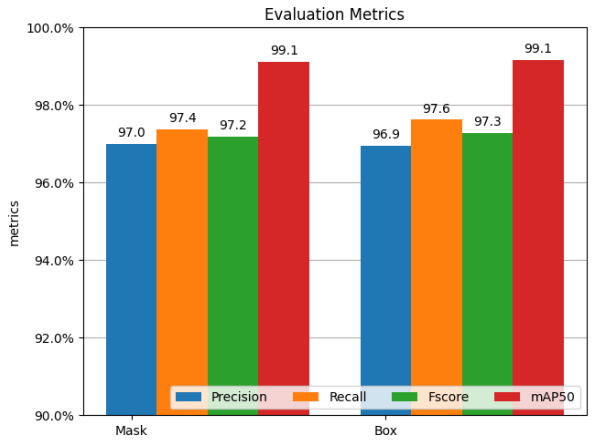

Figure 5: Visualization of evaluation metrics of the segmentation model

3. Results

3.1 Segmentation model results

The research employed the YOLOv8m-seg model for performing image segmentation. This model not only generated mask predictions but also provided bounding box predictions. The dataset employed in this study encompassed two distinct classes, namely PV (Positive Viable) and background. The training outcomes demonstrated the model's strong performance, as evidenced by a notable mask precision value of 0.97 and an impressive mean Average Precision at IoU 50 (mAP50) score of 99.1, (see figure 5).

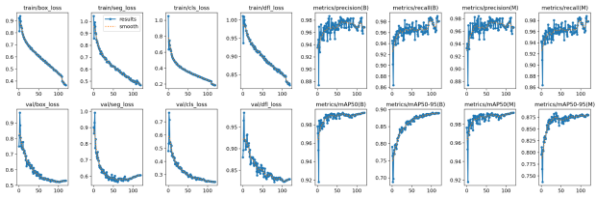

Figure 6: evolution of evaluation metrics across all epochs.

In the evaluation of loss metrics within YOLOv8, various loss functions were employed, including segmentation loss (seg-loss), bounding box loss (box-loss), class loss (cls-loss), and dfl-loss. Among these, the lowest loss value was observed for the class loss (cls-loss), recording at 0.18. This result signifies the model's accurate localization of PV installations. The bounding box loss (box-loss) and segmentation loss (seg-loss) exhibited slightly higher values of 0.36 and 0.46, respectively. Nonetheless, these values remained within an acceptable range and did not significantly impact the overall model performance (see Figure 6).

(figure 11) compares manually annotated polygons. three examples from the test set with corresponding original images, prediction, simplified, and ground truth polygons are shown.

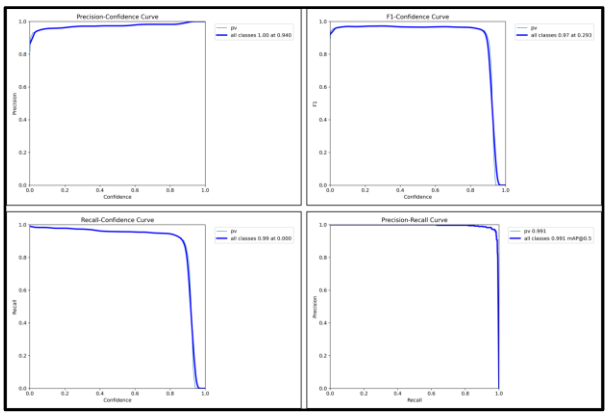

Figure 7: evaluation metrics across range of tresholds.

Throughout the training process, the model employs a range of confidence thresholds spanning from 0 to 1. For each individual threshold, the model computes both precision and recall metrics. Figure 7 illustrates that the model is capable of attaining high levels of precision and recall across a diverse range of confidence thresholds.

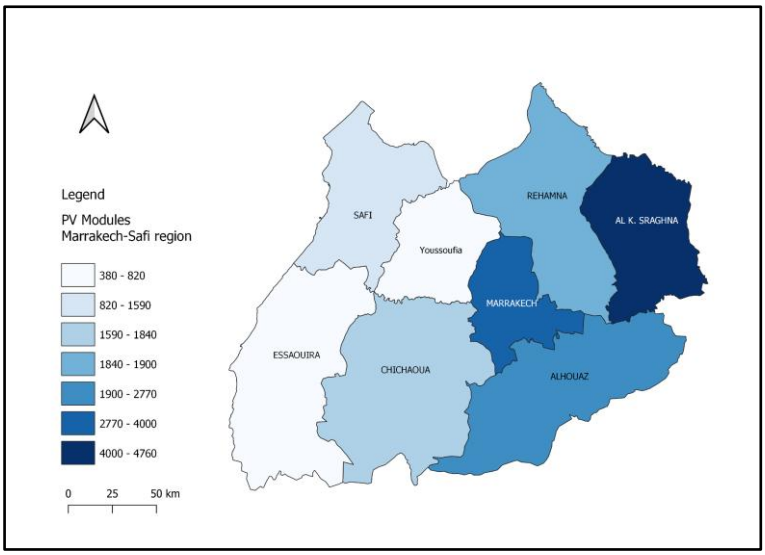

Figure 8: number of segmented PV modules across all provinces of the region.

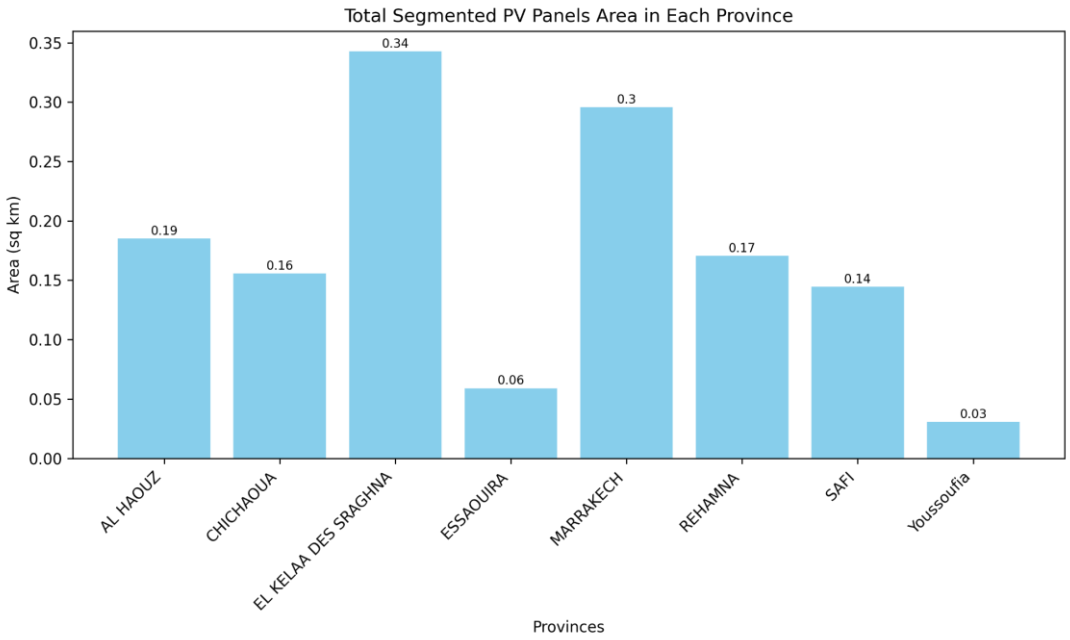

Figure 9: Sum of photovoltaic area by province.

3.2 Geospatial analysis:

Through the implementation of spatial intersection methods, we have effectively linked photovoltaic (PV) installations to their respective provinces, as demonstrated in Figure 8. Notably, EL KELAA DES SRAGHNA exhibits the most substantial count of PV installations, totaling 4763, followed by another notable count of 3996 in the Marrakech province. Conversely, Youssofia records the lowest count of installations at 374. The usage of PV installations differs across regions. In EL KELAA DES SRAGHNA, a majority of the PV installations are employed within the agricultural sector. On the other hand, in the Marrakech region, PV installations find application in both agricultural and residential settings.

The polygons representing the PV installations were transformed to a specific local coordinate system (EPSG:26191). This was done to ensure precise calculations of both the area and perimeter for each installation. As depicted in Figure 9, the combined calculated areas for all installations across different provinces were visualized. As anticipated, EL KELAA DES SRAGHNA showcased the largest total area, measuring 0.34 square kilometers. Following closely, Marrakech exhibited an area sum of 0.29 square kilometers. The provinces of AlHouaz, Rehamna, and

Chichaoua demonstrated slightly similar values, with areas of 0.19, 0.17, and 0.16 square kilometers respectively.

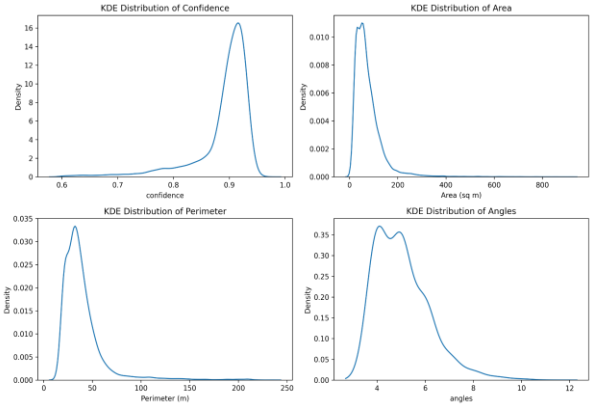

Figure 10: Kernel distribution estimates of PV attributes.

The distribution of estimated parameters is depicted in Figure 10. Notably, perimeter values exhibited their highest density at approximately 50 meters. Similarly, the densities of area values fell within the range of 20 to 150 square meters, with the peak occurring in this interval. The distribution of the number of angles in photovoltaic (PV) installations displayed an equitable spread between four and five angles. Furthermore, confidence levels were recorded, with the maximum density observed at approximately 0.9.

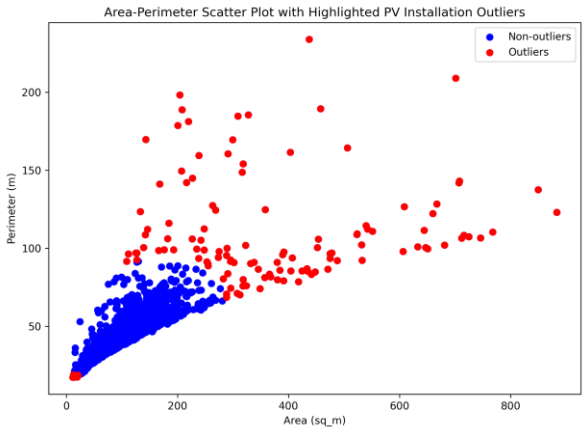

Figure 11: representation of outliers based on area and perimeter.

3.3 Anomaly estimation

Implementing the isolation forest algorithm, we identified outliers within our dataset by considering the attributes of area and perimeter. As shown in Figure 11, a scatter plot was generated to emphasize the data points constituting 5% as outliers. Evidently, the plot reveals the presence of two distinct clusters of outliers, both of which deviate from the overarching data pattern. The first cluster is characterized by notably smaller area and perimeter values, hovering around 10-20 units. Meanwhile, the second cluster predominantly exhibits perimeter values exceeding 100 meters and area values predominantly exceeding 300 square meters.

3.4 Photovoltaic density across LULC classes

To identify the specific application domain of the identified photovoltaic (PV) installations (see figure 12). We performed sample raster values analysis, which allowed us to assign land use and land cover (LULC) classes from the dynamic World V1 dataset of 2022 to the segmented PV modules. In Figure 14, we can observe the distribution of PV installations across various LULC classes. Notably, crop areas constitute the most dominant class, followed by built, trees, and barren land. In contrast, the least prominent classes comprise snow-covered areas, grassland, and water bodies.

4. Discussion

Recent studies have shown a notable improvement in using computer vision to detect solar panels, J. Yu et al. (2018) demonstrated one of the most accurate frameworks to map solar panels in a country scale (USA), P. Li et al. (2021) worked on a city scale and investigated the characteristics of PV panel semantic-segmentation from the perspective of computer vision. his results reveal that the PV panel image data has several specific characteristics: high class-imbalance and non-concentrated distribution; homogeneous texture and heterogenous color features, based on his recommendations about Visual features of PV segmentation we successfully mapped PV modules with different visual features from (color, texture, and shape) as shown in figure 15.

Various possibilities for enhancing this domain persist. Among the most trending fields is the prediction of potential energy production in a specific area, incorporating system-specific variables and real-time energy generation forecasts. Future research will focus on evaluating the technical capacity for energy generation from the segmented surface area of solar PV.

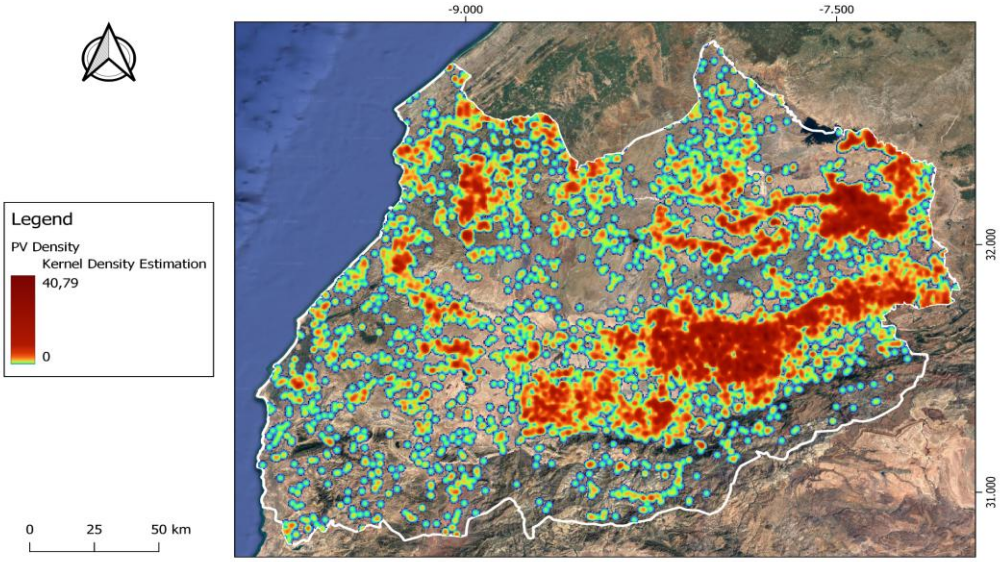

Figure 12: Heatmap illustration for PV panels distribution.

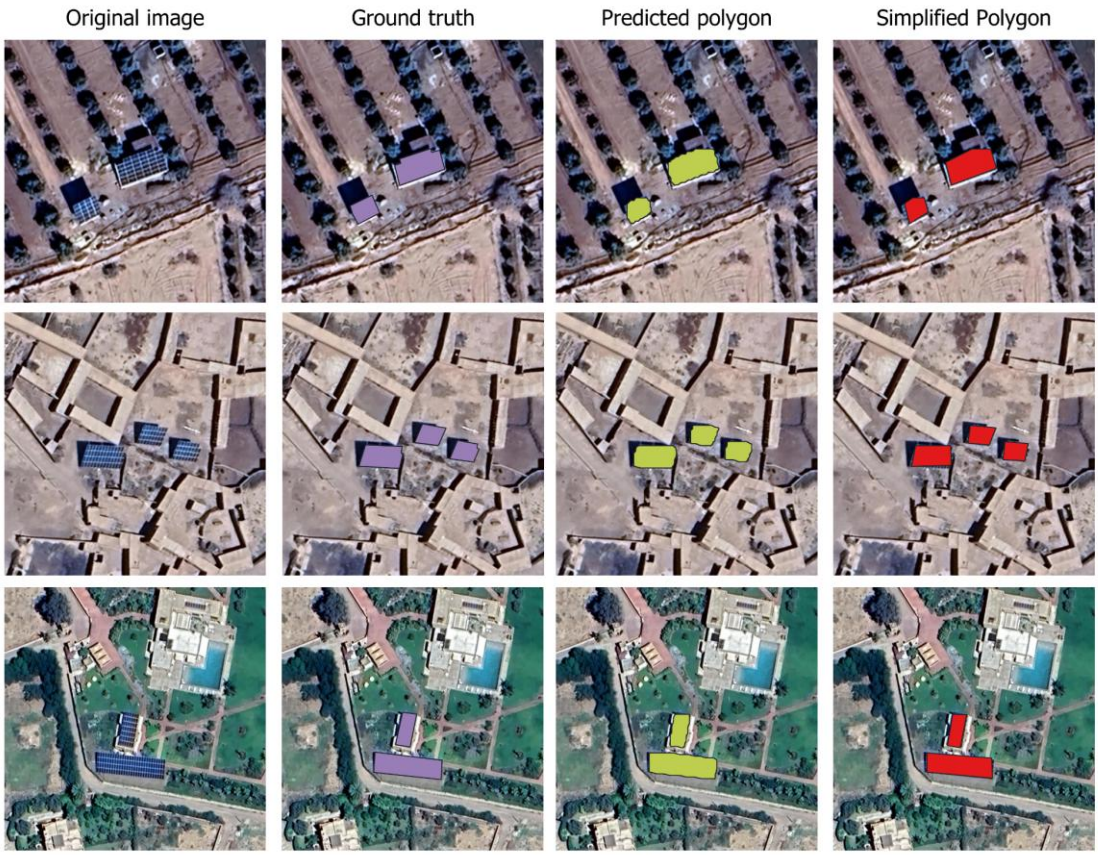

Figure 13: Segmentation results of yolov8(green) compared with ground truth(purple) and simplified polygon(red).

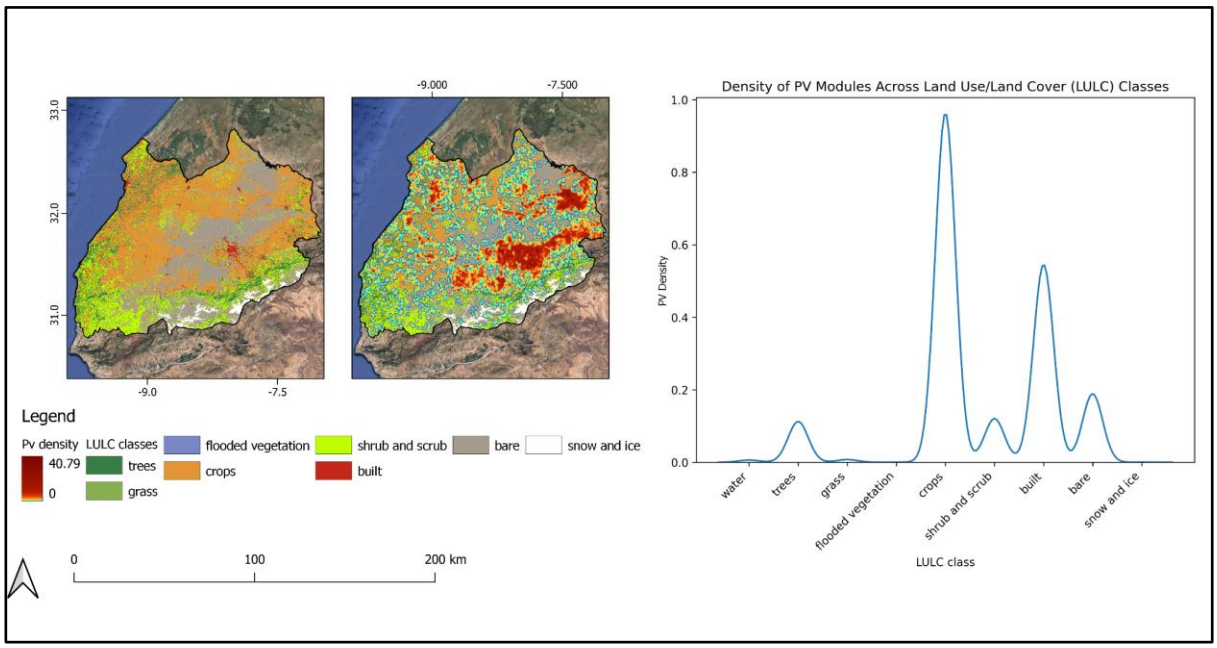

Figure 14: PV panels density for each LULC class.

5. Conclusion

The solar photovoltaic (PV) manufacturing sector has exhibited remarkable growth and has emerged as a significant contributor to energy generation in numerous countries, regardless of the rising costs of raw materials. Nevertheless, the growth of large-scale residential and agricultural solar PV installations has introduced fresh challenges for various stakeholders, including market regulators and power grid operators. A prevalent issue in this context is the lack of comprehensive records detailing the precise locations and capacities of rooftop solar PV systems. To address this challenge, there is a mounting interest in leveraging satellite high-resolution imagery to automate the identification of solar PV system locations and their associated capacities across expansive geographical regions. This paper presents an innovative approach for the precise georeferenced localization and segmentation of solar panels. The outcomes of our study demonstrate the efficacy of the Yolov8 segmentation technique in accurately delineating PV panels from satellite imagery.

These results signify a promising avenue for the development of an automatic, precise, and scalable solution for obtaining critical information regarding PV installations, even in the presence of confusing background surroundings. In future research projects, we intend to refine our methodology by incorporating system-specific factors such as tilt angle, orientation, irradiance levels, and losses due to wiring. This refined approach aims to facilitate the estimation of potential energy output in a given area, further enhancing the utility and relevance of solar PV technology in energy planning and management.

Figure 15: Different visual features of segmented PVs.

Declaration of Competing Interest

The authors declare that they have no known competing financial interests or personal relationships that could have appeared to influence the work reported in this paper

References

Adegun, A. A., Fonou-Dombeu, J. V., Viriri, S., & Odindi, J. (2023). State-of-the-Art deep learning methods for objects detection in remote sensing satellite images. *Sensors*, *23*(13), 5849. https://doi.org/10.3390/s23135849

Advanced data mining techniques. (2008). In *Springer eBooks*. https://doi.org/10.1007/978-3-540-76917-0

Alganci, U., Soydas, M., & Sertel, E. (2020). Comparative Research on Deep Learning Approaches for Airplane Detection from Very High-Resolution Satellite Images. *Remote Sensing*, *12*(3), 458. https://doi.org/10.3390/rs12030458

Brown, C. F., Brumby, S. P., Guzder-Williams, B. P., Birch, T., Hyde, S. B., Mazzariello, J. C., Czerwinski, W., Pasquarella, V. J., Haertel, R., Ilyushchenko, S., Schwehr, K., Weisse, M., Stolle, F., Hanson, C., Guinan, O., Moore, R., & Tait, A. (2022). Dynamic World, Near real-time global 10 m land use land cover mapping. *Scientific Data*, *9*(1). https://doi.org/10.1038/s41597-022-01307-4

Cheng, L., Li, J., Duan, P., & Wang, M. (2021). A small attentional YOLO model for landslide detection from satellite remote sensing images. *Landslides*, *18*(8), 2751–2765. https://doi.org/10.1007/s10346-021-01694-6

Geopandas. (n.d.). *GitHub - geopandas/geopandas: Python tools for geographic data*. GitHub. https://github.com/geopandas/geopandas

Hajjaji, Y., Alzahem, A., Boulila, W., Farah, I. R., & Koubaa, A. (2023). Sustainable palm tree farming: leveraging IoT and Multi-Modal data for early detection and mapping of red palm weevil. *arXiv (Cornell University)*. https://doi.org/10.48550/arxiv.2306.16862

Hong, T., Lee, M., Koo, C., Jeong, K., & Kim, J. (2017). Development of a method for estimating the rooftop solar photovoltaic (PV) potential by analyzing the available rooftop area using Hillshade analysis. *Applied Energy*, *194*, 320–332. https://doi.org/10.1016/j.apenergy.2016.07.001

Jbaihi, O., Ouchani, F., Merrouni, A. A., Cherkaoui, M., Maaroufi, M., & Ghennioui, A. (2021). Site assessment for wet and dry concentrated solar power plant integration using an Analytical Hierarchy Process–Geographic Information System Approach: A case study in the Marrakesh-Safi region. *Energy Technology*, *9*(5). https://doi.org/10.1002/ente.202001135

Li, P., Zhang, H., Guo, Z., Lyu, S., Chen, J., Li, W., Song, X., Shibasaki, R., & Yan, J. (2021). Understanding rooftop PV panel semantic segmentation of satellite and aerial images for better using machine learning. *Advances in Applied Energy*, *4*, 100057. https://doi.org/10.1016/j.adapen.2021.100057

Li, Q., Feng, Y., Leng, Y., & Chen, D. (2020). SolarFinder: Automatic Detection of Solar Photovoltaic Arrays. *2020 19th ACM/IEEE International Conference on Information Processing in Sensor Networks (IPSN)*. https://doi.org/10.1109/ipsn48710.2020.00024

Li, Q., Schott, S., & Chen, D. (2023). SolarDetector: Automatic Solar PV Array Identification using Big Satellite Imagery Data. *International Conference on Internet-of-Things Design and Implementation*. https://doi.org/10.1145/3576842.3582384

Liu, F. T., Ting, K. M., & Zhou, Z. (2012). Isolation-Based anomaly detection. *ACM Transactions on Knowledge Discovery From Data*, *6*(1), 1–39. https://doi.org/10.1145/2133360.2133363

Liu, F., Ting, K. M., & Zhou, Z. (2008). Isolation Forest. *2008 Eighth IEEE International Conference on Data Mining*. https://doi.org/10.1109/icdm.2008.17

Ma, M., & Pang, H. (2023). SP-YOLOV8S: an improved YOLOV8S model for remote sensing image tiny object detection. *Applied Sciences*, *13*(14), 8161. https://doi.org/10.3390/app13148161

Malof, J. M., Hou, R., Collins, L. M., Bradbury, K., & Newell, R. G. (2015). Automatic solar photovoltaic panel detection in satellite imagery. *International Conference on Renewable Energy Research and Applications (ICRERA)*. https://doi.org/10.1109/icrera.2015.7418643

Rasterio. (2013). *GitHub - rasterio/rasterio: Rasterio reads and writes geospatial raster datasets*. GitHub. https://github.com/rasterio/rasterio

Redmon, J., Santosh, D. H. H., Ross, G., & Farhadi, A. (2015). You only look once: Unified, Real-Time Object Detection. *arXiv (Cornell University)*. https://doi.org/10.48550/arxiv.1506.02640

Taha, A. A., & Hanbury, A. (2015). Metrics for evaluating 3D medical image segmentation: analysis, selection, and tool. *BMC Medical Imaging*, *15*(1). https://doi.org/10.1186/s12880-015-0068-x

Terven, J. (2023, April 2). *A comprehensive review of YOLO: from YOLOV1 and beyond*. arXiv.org. https://arxiv.org/abs/2304.00501

Ultralytics. (n.d.). *GitHub - ultralytics/ultralytics: NEW - YOLOv8 🚀 in PyTorch > ONNX > OpenVINO > CoreML > TFLite*. GitHub. https://github.com/ultralytics/ultralytics

Wu, S., & Márquez, M. R. G. (2004). A non-self-intersection Douglas-Peucker algorithm. *16th Brazilian Symposium on Computer Graphics and Image Processing (SIBGRAPI 2003)*. https://doi.org/10.1109/sibgra.2003.1240992

Yu, C., Feng, Z., Wu, Z., Wei, R., Song, B., & Cao, C. (2023). HB-YOLO: an improved YOLOV7 algorithm for DIM-Object tracking in satellite remote sensing videos. *Remote Sensing*, *15*(14), 3551. https://doi.org/10.3390/rs15143551

Yu, J., Wang, Z., Majumdar, A., & Rajagopal, R. (2018). DeepSolar: A machine learning framework to efficiently construct a solar deployment database in the United States. *Joule*, *2*(12), 2605–2617. https://doi.org/10.1016/j.joule.2018.11.021

Zheng, J., Li, Y., & Shi, Z. (2022). LMO-YOLO: a ship detection model for Low-Resolution Optical satellite imagery. *IEEE Journal of Selected Topics in Applied Earth Observations and Remote Sensing*, *15*, 4117–4131. https://doi.org/10.1109/jstars.2022.3176141

Hochberg, M. (2018). Renewable Energy Growth in Morocco: An Example for the Region. 26, MEl Policy Focus 2016.